Direct, Concurrent Measurements of the Forces and Currents Affecting DNA in a Nanopore with Comparable Topography

Edward M. Nelson, Hui Li, and Gregory Timp*

University of Notre Dame, Stinson-Remick Hall, Notre Dame Avenue, Notre Dame, Indiana 46556, United States

ABSTRACT We report direct, concurrent measurements of the forces and currents associated with the translocation of a single-stranded DNA molecule tethered to the tip of an atomic force microscope (AFM) cantilever through synthetic pores with topagraphies comparable to the DNA. These measurements were performed to gauge the signal available for sequencing and the electric force required to impel a single molecule through synthetic nanopores ranging from 1.0 to 3.5 nm in diameter in silicon nitride membranes 6−10 nm thick. The measurements revealed that a molecule can slide relatively frictionlessly through a pore, but regular fluctuations are observed intermittently in the force (and the current) every 0.35−0.72 nm, which are attributed to individual nucleotides translating through the nanopore in a turnstile-like motion.

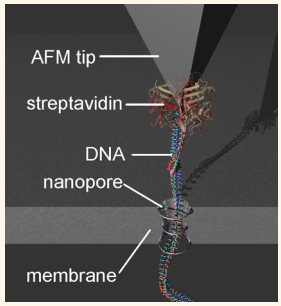

KEYWORDS: nanopore · single-molecule force spectroscopy · AFM · DNA sequencing

To be practical, next-generation DNA sequencing technology will demand single-molecule sensitivity, to eliminate error-prone amplification, and long reads to facilitate the assembly of the genome.[1−3] Nanopore sequencing offers a solution to both problems,[4−7] but single-nucleotide resolution requires stringent subnanometer control over both the DNA configuration in the pore and the translocation kinetics because the equilibrium distance between nucleotides is only 0.35 nm.[8] To gauge the signal available for sequencing and the electric force required to impel a single molecule through a nanopore in a solid-state membrane, direct, concurrent measurements were performed of the forces and currents associated with the translocation of a single-stranded DNA (ssDNA) molecule tethered to the tip of an atomic force microscope (AFM) cantilever. The measurements were accomplished using nanopores with topographies comparable to the DNA ranging from 1.0 to 3.5 nm in diameter in silicon nitride membranes 6−10 nm thick.

These are the first measurements of this type in nanopores small enough to be suitable for sequencing DNA. Early work exploring the forces and current affecting double-stranded DNA (dsDNA)[9,10] or carbon nanotubes (CNT)[11] in synthetic nanopores focused on either pore diameters (>6 nm) that are too large compared to the diameter of DNA for adequate signal for sequencing or voltages that are too small (<125 mV) to suppress translational noise.[12] Very recent work forcing ssDNA into the lumen of a CNT of <3 nm diameter is not easily adapted to sequencing either, because the CNT is too long (10−15 μm) to discriminate single bases in a sequence.[13]

RESULTS AND DISCUSSION

In addition to a topography commensurate with detecting single nucleotides, numerous other technical obstacles had to be overcome to examine the force and current while ssDNA translocates through a nanopore. First, to introduce the ssDNA into the pore, the experimental configuration had to identify the location of the pore unambiguously. Second, since steric considerations do not favor threading ssDNA into a pore, a strategy for guiding the molecule into the lumen repeatedly had to be developed. Finally, this strategy also had to guarantee that only one molecule entered the pore.

* Address correspondence to gtimp@nd.edu.

Received for review October 13, 2013 and accepted May 19, 2014.

Published online May 19, 2014
10.1021/nn405331t

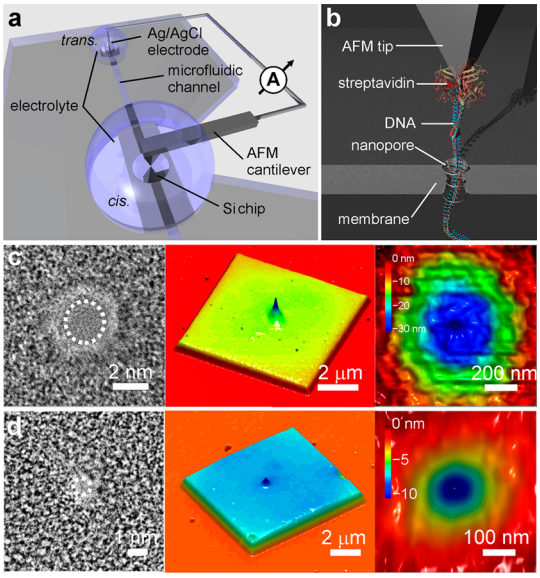

Figure 1. Experimental configuration. (a) Schematic representation of the apparatus used to measure the force and current associated with ssDNA in a nanopore. A silicon nitride membrane with a nanopore in it is bound to a two-layer (*cis/trans*) microfluidic device made from PDMS. An electrical bias is applied between a Ag/AgCl electrode embedded in the *trans*-channel, and the current is measured using an amplifier connected directly to the cantilever holder. (b) Cutaway of the schematic showing biotinylated ssDNA (btssDNA), tethered to the AFM tip through a bond to streptavidin, translocating through the pore. (c) TEM (left) and AFM micrographs (center and right) of a 2.1 nm diameter pore in an 8 nm thick nitride membrane. The shot noise associated with transmission through the pore is highlighted by the white dashed ellipse in the TEM micrograph. (d) TEM (left) and AFM micrographs (center and right) of a 1.0 nm diameter pore in an 8 nm thick nitride membrane. The shot noise associated with the pore is highlighted by the white dashed circle in the TEM micrograph.

To overcome these obstacles, an experiment was configured (Figure 1a,b) that used a customized AFM to simultaneously measure the force and the blockade current. First, an AFM topographical scan with a sharp (nominally 2 nm radius), unfunctionalized tip was used to locate the pore in air relative to fiducial marks, *i.e.*, the edges of a small-area membrane <8 μm on edge (Figure 1c,d). Subsequently, a second AFM cantilever, functionalized with ssDNA, was clamped into the cantilever holder. The cantilever and membrane were then immersed in electrolyte, a trans-membrane voltage bias was applied using Ag/AgCl electrodes, and the pore current was measured with either a trans-impedance amplifier integrated into the cantilever holder or an external amplifier. The pore location was then reacquired through triangulation from the fiducial marks. The electric field that develops when a voltage is applied facilitates capturing the molecule in the pore as the tip is advanced toward it. Indications of the capture appeared in both the current and force measurements simultaneously. Finally, the force on the molecule in the pore was inferred from the cantilever deflection, while the position of the molecule was determined by accounting for both the deflection and the *z*-height above the membrane. The force and current through the pore were recorded while the tip was advanced toward the membrane (3′ direction) and retracted (5′ direction) repeatedly without the molecule vacating the pore. Before retracting to a height above the surface corresponding to the length of the molecule, the direction of the tip was reversed to repeat the measurements.

A blockade of the electrolytic current through the pore, associated with the volume occluded by translocating ssDNA, provided an unambiguous signature of the number of molecules trapped there (Figure 2). In support of this claim, a series of experiments were performed to characterize the blockade current associated with ssDNA and dsDNA in nanopores of comparable diameter. When 20 pM, 5 kbp dsDNA is introduced into the electrolyte at the negative (*cis*) electrode and a 0.4 V bias is applied across the membrane, transients like that shown by the red trace in Figure 2a (left) are observed in the current through a nanopore with a 2.1 $\times$ 2.7 nm cross-section. The distribution of transients observed can be represented by a blockade with a single peak centered at $\Delta I = I - I_0 = 330 \pm 25$ pA, where I_0 represents the open pore current. If the duration of the blockade corresponds to the interval when a single 5 kbp dsDNA occupies the pore (the observed interarrival time ~1 min), then the average transient width $t_D = 80.2 \pm 5.3$ ms at 0.4 V signifies the time required to translocate through it, which is slower than other estimates.[14−16]

To extend the dwell time in the pore and facilitate low-noise measurements of a current blockade, the biotinylated 5′ ends of ssDNA and dsDNA were bound to the streptavidin tetramer (SA) that was, in turn, trapped by the electric field in the nanopore (see inset in Figure 2a; SA has a molecular weight of ~60 kDa with a 105−133 nm^3 volume estimated by AFM).[17] In contrast with the 5 kbp dsDNA, measurements of the blockade current associated with streptavidin-biotinylated-(SA-bt-ssDNA) in the same nanopore revealed a shallower blockade of longer duration. One example is shown by the red trace in Figure 2a (left); the blockade measured at 0.4 V associated with a 150-nt poly(T)$_{150}$ molecule has a value of $\Delta I = 180.7 \pm 20.2$ pA with a current transient that exceeds 2 s in duration. (On the other hand, if a biotinylated strand of dsDNA is bound to SA and trapped in the pore, due to the action of the field, it melts apparently into a single strand, presumably the biotinylated one, as evident from the observed change in blockade current from a value consistent with dsDNA for <50 ms to one consistent with ssDNA for longer times; data not shown.)

It is also possible to distinguish a single strand from multiple strands trapped in the pore over a wide voltage range. The voltage dependence of the blockade currents, ΔI, associated with 5 kbp dsDNA and

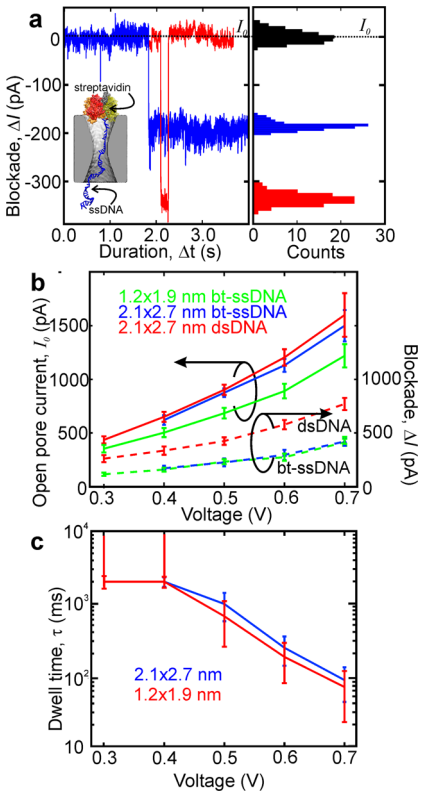

Figure 2. Single-molecule blockade current and dwell time measured for biotinylated ssDNA in nanopores. (a, left) Electrolytic current measured in 100 mM KCl as a function of time through the 2.1 × 2.7 ± 0.2 nm cross-section pore sputtered through a nominally 10 nm thick silicon nitride membrane at 0.4 V. The figure compares (red trace) a typical current transient associated with 5 kbp dsDNA translocating through the pore with the blockade current trace of a trapped complex (blue trace) of streptavidin−bt-ssDNA. (a, right) Histograms showing the corresponding distribution of the blockade currents for >100 events each. Inset: Schematic of streptavidin-btssDNA trapped in a nanopore. (b) Voltage dependence of the open pore, I_0, and blockade current, ΔI, associated with biotinylated poly(T)$_{150}$ (bt-ssDNA) trapped in nanopores with 1.2 × 1.9 and 2.1 × 2.7 nm cross-sections. For comparison, I_0 and ΔI associated with 5.0 kbp dsDNA are shown for the 2.1 × 2.7 nm cross-section only. At the same voltage, the blockade current associated with bt-ssDNA is the same for the two different cross-section pores because the occluded volume is the same. However, at the same voltage and open-pore current, the blockade due to the ssDNA is only about half of that associated with the dsDNA. (c) Voltage dependence of the dwell times inferred from the blockade current measured for streptavidin-bound biotin-ssDNA in two pores of (b). The dwell time exceeds 100 ms for $V < 0.7$ V and is interminable for $V < 0.4$ V.

bt-ssDNA measured after the molecule was trapped for a long duration in the same pore is plotted in Figure 2b along with the open-pore current, I_0. It was observe that, within the measurement error, the blockade current for bt-ssDNA was always smaller than the current associated with dsDNA. Moreover, the blockades attributed to ssDNA were relatively independent of the pore geometry for nominally the same membrane thickness, indicating that the blockade measures mainly the occluded volume in the pore. On the basis of data like this, blockade currents in the range $114 < \Delta I < 420$ pA were associated with a single ssDNA strand trapped in 1.2−2.7 nm diameter pores for voltages in the range $0.3 < V < 0.7$ V, respectively.

Parenthetically, in contrast with the dwell time measured for 5 kbp dsDNA, the duration of the blockade associated with the SA complex trapped in the pore was extended significantly; that is, τ is an exponentially decreasing function of the applied voltage (Figure 2c). Consistent with the drift of the tip relative to the location of the nanopore, the longer dwell time translates to higher signal-to-noise in the current measurement generally, but demands loading the SA−biotin bond for a longer duration. Furthermore, at low voltage (≤0.4 V) the duration of a blockade associated with the complex is interminable; the blockade usually ends only if the voltage is manually reversed, impelling the complex out of the pore, allowing for quasi-static measurements of the force and current. Whereas these long duration blockades in a nanopore at constant force are not unprecedented,[17] they were long in comparison to extrapolations from dynamic force measurements of the SA−biotin bond by an AFM[18−20] and suggested that the load on the trapped DNA may be shared between the membrane and the SA−biotin bond.

Force and current measurements (coincident within 0.1 ms; Figure S1 in the Supporting Information) performed with a 150-mer homopolymer of thymine, poly(T)$_{150}$, tethered to the tip (Figures 3, 4) revealed several interesting features. For example, the force measured as the cantilever was extended toward a 2.1 ± 0.2 nm nanopore (Figure 1c) at a constant velocity of 20.00 ± 0.02 nm/s against a potential of 0.5 V (Figure 3a,b) revealed a force plateau during the translocation of a single molecule. Generally, these nanopores had a biconical topography with about a 20° cone angle in membranes that ranged from 6 to 10 nm thick.[21] Finite-element simulations (FES) of pores with this topography revealed that the electric field was tightly focused in the pore,[22,23] peaking at 8×10^5 V/cm near the center of the membrane for this voltage bias and decaying to 4×10^4 V/cm 10 nm above the opening (Figure S2 in the Supporting Information). Accordingly, at position 1, where the gap between the membrane and the tip apex is 8.3 nm, the molecule was pulled toward the pore with a force of 13.8 ± 0.4 pN due to the electric field that extends out of the pore some distance above the membrane,[22] without an appreciable effect on the current. However, as the tip apex approached within 7 nm of the membrane at position 2, the ssDNA was captured by the field inside the nanopore since the current abruptly changes, $\Delta I = 240 \pm 60$ pA, whereas the force on the molecule remains about the same until the tip makes contact with the membrane.

Constant force plateaus like that observed in Figure 3a were interpreted as the molecule sliding

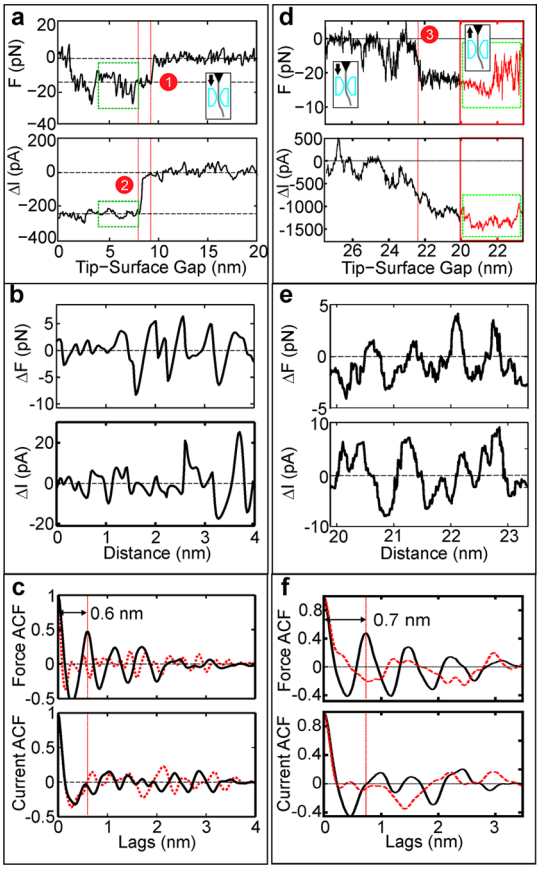

Figure 3. Simultaneous direct measurements of the force and current as ssDNA translocates through a nanopore. (a) Force (top) on poly(T)$_{150}$ and the ionic blockade current (bottom) under an applied potential of 0.5 V measured while the AFM cantilever was extended toward the nanopore at 20.0 nm/s in 100 mM KCl, showing a relatively frictionless plateau in the force. Inset: Assumed molecular configuration with the arrow indicating the direction of the cantilever motion. (b) Magnified view of the force (top) and current (bottom) highlighted in (a). (c) Corresponding ACF of the force (top) and current (bottom) from the signals in (b) (black), respectively, along with the ACFs from the signal with no DNA in the pore (red). Features are observed regularly in the force with a 0.62 nm periodicity. (d) Like (a), the force (top) and blockade current (bottom) measured as poly(T)$_{150}$ was inserted into (black) and extracted from (red) a 1.0 nm diameter pore at a 1.00 nm/s rate against an applied potential of 0.45 V. The green box highlights a 3.5 nm portion of the data in which the ACFs were calculated. Insets: Assumed molecular configuration with the arrow indicating the direction of the cantilever motion. (e) Change in force (top) and blockade current (bottom) measured by lock-in detection corrsponding to the highlighted range in (d). (f) Corresponding ACFs of the force (top) and current (bottom) respectively of the traces in (e) along with the ACFs from the signal with no DNA in the pore (red).

relatively "frictionlessly" through the pore. Plateaus in the force were observed also without ssDNA in the nanopore as the molecule was peeled from the surface of the membrane (Figure S3 in the Supporting Information). Such plateaus have been reported when ssDNA is peeled from gold[24] or graphite[25] surfaces and when ssDNA is extracted from the lumen of a CNT.[13] While conformational changes in ssDNA may produce a force plateau also,[24] thymine homopolymers

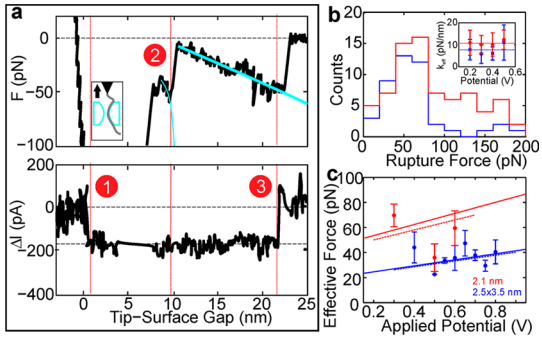

Figure 4. Translocation kinetics through a nanopore. (a) Like Figure 3a, the force (top) and current blockade (bottom) observed under an applied potential of 0.5 V while the AFM cantilever was retracted from the pore at 20.0 nm/s in 100 mM KCl showing a typical loading of a single molecule that produces a force–extension curve reflecting the molecular elasticity. The blue lines represent fits to the FJC model for each individual stretch. (b) Rupture force of stretched poly(T)$_{150}$ for a nanopore with a 2.1 nm diameter in 100 mM KCl at various applied potentials when there was a molecule in the pore as evident by the observation of a simultaneous blockade in the current (blue) and when there was no molecule in the pore (red). Inset: Effective spring constant as a function of applied potential of poly(T)$_{150}$ for the events in (b). (c) Compilation showing the value of the force plateau when poly(T)$_{150}$ is sliding through a 2.5 × 3.5 nm pore (blue) or a 2.1 nm diameter pore (red) as a function of applied potential. The dashed lines are fits to the data, with a nonzero intercept at $V = 0$, which account for both the electrophoretic force and electro-osmotic flow.

possess only minimal secondary structure.[26] Here, the force plateau may be associated with a combination of a relatively weak ($W < F\Delta l = 9.7 \times 10^{-20}$ $J \cong 5$ kJ·mol^{-1} base^{-1}) hydrophobic adhesion between the bases and the silicon nitride surface, the electrophoretic force, and the electro-osmotic flow impelling the molecule through the pore (Figure S2 in the Supporting Information).[27]

Importantly, the force associated with the plateau fluctuates above the estimated minimum force noise (see Materials and Methods). Close inspection of the force and the current (Figure 3b) revealed regular fluctuations intermittently with the peaks spaced nearly equidistant. The periodicity was more apparent in the autocorrelation function (ACF) of the data where the force exhibited regular oscillations (Figure 3c, top, black) at a mean lag of 0.62 ± 0.08 nm in contrast to ACFs obtained without a molecule in the pore (red traces), which show no regular pattern. The mean spacing between peaks without a molecule in the pore ($|dz|_{force}$ = 0.27 ± 0.06 nm) was consistent with white noise ($|dz|_{noise}$ = 0.24 ± 0.13 nm). Fluctuations in the current with a similar period were not perceptible above the noise in this case.

To improve the signal-to-noise ratio, smaller pore diameters were investigated. Figure 3d shows force and current measurements obtained as poly(T)$_{150}$ was consecutively inserted and extracted against a 0.45 V trans-membrane potential at a constant velocity of 1.00 ± 0.01 nm/s through a pore with a 1.0 nm

diameter (Figure 1d). As the molecule was inserted into the pore at a tip height of about 22 nm above the surface, a force plateau was observed at 12.7 ± 4.7 pN starting at position 3, indicating a molecule was trapped in the field of the pore. The force plateau corresponds to an exaggerated blockade current of $\Delta I = 1.2 \pm 0.2$ nA, which can only signify one molecule trapped in the pore due to the small diameter. A magnified view of the force and blockade current (Figure 3e) measurements accomplished using lock-in detection again revealed regular fluctuations; the periodicities were apparent in the ACFs of the data (Figure 3f). In this case, both the force and current exhibited regular oscillations (black traces) at a mean lag of 0.72 ± 0.01 nm. The separations between peaks in the force and current ACFs were nearly equidistant over the 3.5 nm range from which the ACF was obtained.

The regular patterns observed in the force and blockade current were consistent with a turnstile motion of consecutive nucleotides through the pore in which the translocation stalls repeatedly in a well-defined conformation. Sigalov *et al.*[8] predicted such a turnstile motion for the translocation kinetics of ssDNA with a periodicity of 0.75 nm every time a nucleotide entered the narrowest part of the 1 nm diameter biconical pore. Due to a combination of geometrical constraints in the pore and the applied electric field, for each translocation direction the average density of bases becomes localized precisely at the 1 nm entrance to the constriction near the center of the membrane because the progress of the nucleotide was interrupted until a sufficient force was applied to stretch, reorient, or tilt the base and impel it through. The concomitant reorientation and tilting of the partial charges in the DNA should present a distinctive change in the energy barrier to the flow of ions that is reflected in the blockade current as well. Thus, according to this argument, the fluctuations in the force and current observed during a translocation reflect variations in the mobility of an ssDNA molecule due to changes in the topology and orientation of nucleobases in the pore.

The regularity of the fluctuations suggests a correlation between the orientation and topology of the bases in the pore. Interestingly, these membranes ranged from 6 to 10 nm thick, such that at least 10 nucleobases were in the pore during a transit, which further suggests that the correlations extend over several bases. Sigalov also predicted that the spacing between nucleobases would be correlated with the standard deviations in the average distances between the location of the nth nearest neighbor phosphates, increasing from 0.05 nm for $n = 1$ to 0.25 nm for $n = 5$.[8] Thus, the peaks in the ACF extracted from the force and current fluctuations were expected to be nearly equidistant. Taken altogether, these data indicate that the translocation of a nucleotide through the constriction in a biconical pore on a frictionless force plateau occurs in steps that are subject to control by the applied force.

An entirely different category of kinetics is depicted in Figure 4a, which shows the force and current measured as the cantilever was retracted from the 2.1 nm diameter pore (Figure 1c) under the same conditions as in Figure 3a. At tip−surface separations of <5 nm, the adhesion between the tip and the silicon nitride membrane predominated. Just as the tip was released from the surface at position 1, a single ssDNA was observed to occlude the pore, giving rise to a blockade $\Delta I = 166 \pm 25$ pA. The ssDNA, which was likely bound to the surface of the membrane, was stretched until the bond ruptured at position 2. This process was repeated until the final bond ruptured at position 3 with a force of 46.2 pN, when the molecule vacated the pore and the current returned to the open pore value.

Stretching events like these in this force range can be described by a freely jointed chain (FJC) model using a Kuhn length of $b \approx 1.5$ nm.[28,29] The effective spring constant associated with each stretching event was estimated from $k_{eff} = 3k_BT/bX$, where k_BT represents the thermal energy at 293 K and X is the extension of the ssDNA relative to its total length (blue lines) to find $k_{eff} = 6.4 \pm 3.6$ and 3.4 ± 2.1 pN/nm at positions 2 and 3, respectively, which is consistent with prior estimates.[28] At a constant extraction velocity of 17.86 ± 0.02 nm/s, these spring constants imply loading rates of 115 and 60.3 pN/s, respectively, indicating a near-equilibrium loading regime and a single bond type.[30−32]

Usually, the loading of a single molecule produces a force−extension curve that reflects the elasticity of the molecule like that shown in Figure 4a.[31] The associated kinetics through the pore resemble a "stick−slip" motion in which the polymer rapidly exits as soon as the applied force exceeds the threshold for rupturing the adhesive bond between the nucleotides and the membrane. Two pieces of evidence relating to the rupture force and spring constant support the "stick−slip" interpretation of the motion. First, measurements of the rupture force obtained by pulling poly(T)$_{150}$ from the pore (Figure 4b, blue histogram) and the force required to pull the molecule off the surface of the nitride membrane (Figure 4b, red histogram) show comparable values near 60 pN. (Sample force curves are shown explicitly in the supplemental Figure S4 in the Supporting Information.) Second, the elastic energy of the stretched ssDNA shows only a weak dependence on the applied potential (Figure 4b, inset).

Incidentally, the complex interactions of DNA with the flowing electrolyte in a nanopore can be decomposed into two independent motions: one motion is that of DNA dragged at a constant velocity v by a nonelectric force $F = \xi v$; and the other is that of DNA drifting in an electric field E with a constant velocity $v = \mu E$, where ξ and μ are the friction coefficient and

electrophoretic mobility, respectively.[33,34] Thus, the zero-voltage intercept in Figure 4c cannot be used to estimate the size of the nonelectric force unambiguously because the nonelectric force has a different origin and must be measured by another means. Moreover, the effective force on a single molecule sliding through a nanopore larger than ssDNA depends weakly on the applied potential with a slope, *e.g.*, $\Delta F/\Delta V = 23 \pm 90$ pN/V for a pore with a 2.5 $\times$ 3.5 nm cross-section (Figure 4c), which is in contrast with the result reported by Keyser *et al.* ($\Delta F/\Delta V = 240 \pm 20$ pN/V) obtained using duplex DNA in much larger pores through much thicker membranes.[10,33,34] Remarkably, FESs of the effective force as a function of applied potential (Figure S2e in the Supporting Information) in this topography indicated that the electro-osmotic effect nullifies up to 95% of the electrophoretic force in a 6 nm diameter pore in a 8 nm thick membrane. However, for smaller diameters, the topography and the corresponding lack of water in the pore[27] reduces the electro-osmotic effect.

A typical data set of 280 force curves produced only 24 events in which the current was affected concurrently, of which 11 were considered frictionless, whereas the same data set contained 13 "stick–slip" force curves with concurrent blockades, six of which were single rupture events. After the baseline stretching force was subtracted, the fluctuations in the force–extension curves attributed to "stick–slip" kinetics were analyzed. However, the residual forces and the corresponding current blockades associated with single poly(T)$_{150}$ stretching in a pore did not exhibit regular, correlated fluctuations like those observed on frictionless plateaus (Figure 3). On the other hand, a careful analysis of the force and current fluctuations observed in the subset of measurements obtained when a single poly(T)$_{150}$ translocated through a pore on a frictionless force plateau revealed regular correlated patterns intermittently (Figure 5). Figure 5a shows typical force and current measurements obtained as the cantilever was retracted against 0.3 V at a constant velocity of 19.585 $\pm$ 0.001 nm/s through a pore with 2.1 nm diameter (Figure 1c). As the tip is retracted, initially at position 1 a blockade current of $\Delta I = 103 \pm 9$ pA was observed, which likely signifies more than one molecule in the pore. Subsequently, at position 2, a force plateau is observed at 78.6 $\pm$ 2 pN, corresponding to a blockade of $\Delta I = 60 \pm 17$ pA, which was attributed to a single molecule loading the tip. Finally, at position 3, the force was relieved while the current remained blockaded before returning to the open-pore value at position 4. Since the current returned to the open pore value after the force was relieved, it was inferred that the SA–biotin bond ruptured prematurely and the molecule remained for an additional ~250 ms before the biotinylated DNA vacated the pore.

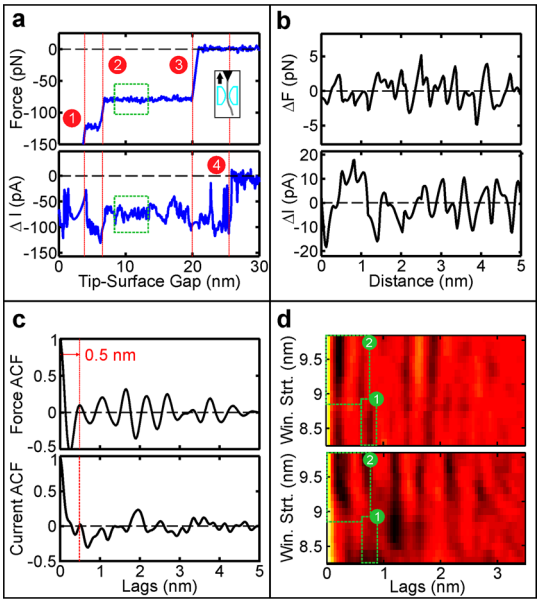

Figure 5. Force and current associated with an ssDNA homopolymer sliding through a pore on a force plateau. (a) Force (top) and blockade current (bottom) measured as poly(T)$_{150}$ is extracted at 19.66 nm/s from a 2.1 nm diameter pore against an applied potential of 0.3 V. The green box highlights a 5 nm portion of the data in which the ACF is calculated. The cartoon shows the assumed molecular configuration with the arrow indicating the direction of the cantilever motion. (b) Magnified view showing the change in force (top) and blockade current (bottom) of the highlighted data. (c) Corresponding ACFs of the force (top) and current (bottom), respectively, of the traces in (b). (d) Kymographs of the force and current (top, bottom), respectively, representing a compilation of traces similar to (c) obtained with a 3.5 nm window, but with a staggered start. The lag between peaks in the ACF shifts 0.1 nm between regions 1 and 2, highlighted in white.

A magnified view of the force and blockade current (Figure 5b) revealed regular fluctuations; the periodicities were apparent in the ACFs of the data (Figure 5c). According to Figure 5c, both the force and current exhibited regular oscillations (black traces) at a mean lag of 0.53 $\pm$ 0.05 nm. The separation between peaks in the force and current ACFs was nearly equidistant over the 5 nm range from which the ACF was obtained, but over a smaller window the peaks were found to shift, as evident from the kymographs (Figure 5d), which represent a compilation of ACFs using a 3.5 nm moving window with a starting position that is staggered by 0.1 nm, which corresponds to 50$\times$ the sampling frequency. About a 0.1 nm shift in the position of the ACF peaks was evident between regions 1 and 2.

From the perspective of sequencing, an analytical tool with long read lengths that can count repetitive segments would be invaluable, as it becomes exponentially harder to assemble a genome as the number of repeats grows.[1,2] To test the prospects for detecting repeats, a subset of data obtained on a force plateau when a single heteropolymer poly(C_4A_4)$_{20}$ slid through a pore (Figure 6a) was identified and the fluctuations there were analyzed similarly. It was reasoned that the

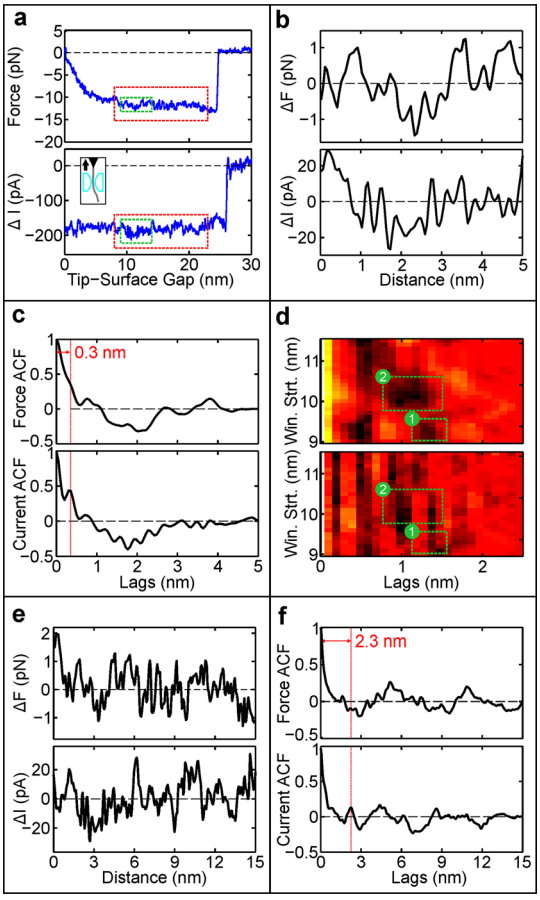

Figure 6. Force and current fluctuations associated with an ssDNA heteropolymer sliding through a nanopore on a frictionless force plateau. (a) Force (top) and blockade current (bottom) measured as poly(C_4A_4)$_{20}$ is extracted at 20.75 nm/s from a 1.4 × 1.6 nm^2 cross-section pore against an applied potential of 0.4 V. The green and red boxes highlight a 5 and 15 nm portion of the data, respectively, from which the ACFs were calculated. The cartoon shows the assumed molecular configuration with the arrow indicating the direction of the cantilever motion. (b) Magnified view showing the change in force (top) and blockade current (bottom) in the 5 nm window. (c) Corresponding ACFs of the force (top) and blockade current (bottom) obtained from the data in (b). (d) Kymographs representing a compilation of ACFs for the force (top) and current (bottom) obtained using a 2.5 nm window in the 5 nm region highlighted in (a) with staggered starting positions. (e) Magnified view showing the change in force (top) and blockade current (bottom) in the 15 nm window in (a). (f) ACF of the force (top) and the blockade current (bottom) of the signal in (e).

difference in size between a purine (A) and pyrimidine (C), and nucleobase mobility differential,[8] would facilitate discrimination. Figure 6 shows a typical result acquired when a single molecule was extracted from a 1.4 × 1.6 nm^2 cross-section pore (Figure S5a−c in the Supporting Information) against a potential of 0.4 V at a constant velocity of 20.75 ± 0.02 nm/s. Associated with the force plateau at 11 ± 1 pN, a blockade of ΔI = 225 ± 10 pA was observed, which was consistent with a single ssDNA occluding the pore (Figure 6a). An analysis of the fluctuations in the force and blockade (Figure 6b) over a 5 nm window revealed regular fluctuations with a mean lag of 0.30 ± 0.01 nm in the current, whereas the fluctuations with the same periodicity found in the force were inconclusive (Figure 6c). A moving 2 nm window with a starting position that is staggered by 0.1 nm (Figure 6d) exhibited a persistent 0.3 nm period in the current data, whereas the force ACF shifts about 0.2 nm, which may account for the obfuscation of the periodicity in a longer 5 nm window. Furthermore, analysis with a 15 nm window (Figure 6e) showed that the 0.3 nm period was modulated. The current ACF displayed a maximum near 2.3 nm (Figure 6f), which was consistent with the chemical constituency of the heteropolymer, *i.e.*, for C_4A_4 0.3 nm × 4 × 2 = 2.4 nm. Moreover, for a lag of >4 nm, both the force and the current ACFs showed regular patterns consistent with the C_4A_4 structure. While the fluctuations viewed through the ACFs are emblematic of a heteropolymer, the force and current differences between A and C are minute (<1 pN and <20 pA, respectively) and difficult to identify under these conditions. Thus, without an improvement in the postacquisition signal recovery,[35,36] it would be difficult to unambiguously discriminate A from C with single-nucleotide resolution.

CONCLUSIONS

Direct, concurrent measurements of the forces and currents associated with the translocation through a nanopore of an ssDNA tethered to the tip of an AFM cantilever were performed to gauge the signal available for sequencing and the electric force required to impel a single molecule through synthetic nanopores. These measurements revealed two types of translocation kinetics: frictionless sliding and "slip−stick" motions. On a force plateau associated with the molecule sliding through the pore, regular patterns were observed intermittently in the force and current separated by 0.3−0.72 nm in both homopolymers and heteropolymers, which were consistent with the equilibrium spacing between partially stretched nucleotides. For the heteropolymer, this periodicity is modulated by a regular pattern with a 2.3 nm period, consistent with its chemical constituency, which supports the notion that sufficient resolution can be developed in a synthetic nanopore to identify individual bases, but with difficulty in pores with a diameter of >1.5 nm.

MATERIALS AND METHODS

Nanopore Fabrication. To create a single nanopore, a silicon nitride membrane was sputtered by using a tightly focused, high-energy (300 kV) electron beam in a scanning transmission electron microscope (STEM, Titan 80-300, FEI, Hillsboro, OR, USA). Typically beam currents ranged from 0.5 to 1.2 nA,

resulting in pores that ranged in diameter from 1.2 to >4 nm after 10−30 s of sputtering. Transmission images of the sputtered pore were obtained from the microscope in TEM mode. The thickness of the membranes, which ranged from 6 to 10 nm, was measured *in situ* using electron energy loss spectroscopy prior to sputtering. The topography of the pore was modeled as biconical, with a cone angle determined by tilting the membrane relative to the beam.[21]

Microfluidics and Electrical Characterization. The silicon chip supporting a silicon nitride membrane with a nanopore in it was bonded to a polydimethylsiloxane (PDMS, Sylgard 184, Dow Corning) microfluidic device as described elsewhere.[22] The microfluidic devices consisted of a microchannel (250 μm × 75 μm) configured to independently address the *cis*-side of the membrane through a 250 μm wide channel. Prior to mounting, the chips were cleaned in a piranha etch solution (H_2SO_4/H_2O_2,1:3) for 10 min. Because the mixture is a strong oxidizer, it hydroxylates most surfaces by adding OH^- groups, making them hydrophilic. The membrane with a pore in it was rinsed subsequently in 18 MΩ deionized water several times over 10 min. Next, the transparent microfluidic device was plasma bonded (PDS-001, Harrick Plasma, Ithaca, NY, USA) simultaneously to the silicon chip and a clean glass slide to gain optical access through the bottom (on the *trans*-side). To ensure the seal of the microfluidic device, the top and edges of the silicon chip were coated with a thin layer of PDMS, and then the ensemble was cured at 120 °C for 5 min. Finally, the microfluidic device was rigidly clamped to the AFM scanner stage on an inverted optical microscope (Axio-Observer Z1, Frankfurt Germany).

To characterize the pore, a trans-membrane voltage was applied using Ag/AgCl electrodes (Warner Instruments, Hamden, CT, USA) embedded in each side of a microfluidic device, and the corresponding current was measured at 17 ± 0.1 °C using an Axopatch 200B amplifier with the output digitized with a DigiData 1440 data acquisition system (DAQ, Molecular Devices, Sunnyvale, CA, USA) at a sampling rate of 100 kHz for subsequent analysis. A BNC-2090-series DAQ card (National Instruments, Austin, TX, USA) was used, in conjunction with a custom LabVIEW program (v2009, National Instruments), to control the electrode voltage.

To quantify the blockade current associated with ssDNA, a complex consisting of biotinylated poly(T)$_{150}$, (IDT, Coralville, IA, USA) bound to stretpatvidin (S4762, Sigma-Aldrich) was trapped by the electric field in the pore. The biotinytated-ssDNA at a concentration of 20 pM was mixed with streptavidin at the ratio 1:10 in a 100 mM KCl solution supplemented with 10 mM Tris (pH 8.0) for 1 h at 23 °C. In addition, the blockade current associated with 5 kbp dsDNA (NoLimits, Thermo Scientific) was measured in the same pore under the same conditions. The data were analyzed with customized MATLAB (v2010a, Natick, MA, USA) and Clampfit (v10.2, Molecular Devices) software. Open-pore and blockade currents from >100 events were fit to a Gaussian distribution to extract I_0 and ΔI, respectively, whereas the average duration of the blockade was determined by fitting a log-normal function to the dwell times.

Force Spectroscopy with an Atomic Force Microscope. The force and current data were obtained on a customized AFM (MFP-3D-BIO, Asylum Research, Santa Barbara, CA, USA) interfaced to an inverted optical microscope (Axio-Observer Z1, Zeiss). In particular, the AFM employed a narrow bandwidth filter (850 nm center ± 30 nm pass band with >OD6 out-of-band) for the superluminescent diode in the head and a low-noise Z-sensor coupled with an ultraquiet Z-drive to produce noise at the tip−sample distance of <30 pm at 1 kHz bandwidth. To minimize drift and reduce acoustic noise, the inverted optical microscope was mounted on an optical air table with active piezoelectric vibration control (Stacis, TMC, Peabody, MA, USA), housed in an acoustically isolated, NC-25 (noise criterion) rated room in which the temperature was stabilized to less than ±0.1 °C over 24 h through radiative cooling. Temperature fluctuations appear to be the dominant source of long-term drift, and with temperature regulation the drift of the system was reduced to 600 pm/min. Sound couples strongly in the microscope and is another potential source of instrument noise. Therefore, acoustically loud devices, especially those with cooling fans such as power supplies, amplifiers, and computers, were placed outside the room. With these precautions, force detector noise is <10 pm/$\sqrt{\text{Hz}}$ for frequencies above 1 Hz.

The Z-piezo sensor (Z-sensor) was calibrated using a standard calibration grating (NT-MDT, Moscow, Russia). The deflection sensitivity was calibrated by pressing the tip against a freshly cleaved mica surface and correlating the cantilever deflection to the Z-sensor reading. The spring constant was determined by measuring the thermal noise spectra and fitting the response to a simple harmonic oscillator.[37]

The topography of the silicon nitride membrane and the location of the pore relative to the edges of the membrane were determined in air in noncontact (tapping) mode using a silicon cantilever (SSS-FM, Nanosensors, Neuchatel, Switzerland) with a 2 nm nominal radius, a spring constant ranging from 0.5 to 9.5 nN/nm, and a 45−115 kHz resonant frequency (in air). Force spectroscopy was performed in 100 mM KCl and 10 mM Tris-HCl (pH 8.5) using either contact mode cantilevers (PPP-CONT, Nanosensors) with a 7 nm nominal tip radius, a 0.02−0.8 nN/nm spring constant, and a 6−21 kHz resonance frequency or custom MSNL silicon cantilever (Bruker, Camarillo, CA, USA) without metal reflex with a 2 nm tip radius, 0.005−0.3 nN/nm spring constant, and 4−100 kHz resonant frequency. Considering only the off-resonance thermal noise of the cantilever, $\Delta F_{min} = (4k_BT\Delta f k_{spr}/\omega_0 Q)^{1/2} < 3$ pN, where typically k_{spr} = 5−30 pN/nm, Δf = 100−250 Hz is the measurement bandwidth, $\omega_0 = 2\pi \times 1.2-22.7$ kHz is the angular resonance frequency of the cantilever, and Q = 1−1.5 is the quality factor.

To functionalize an AFM tip, the cantilever was first conditioned in a 20% oxygen plasma at 25 W (Harrick Plasma) for 1 min and then immersed in a 0.1% (v/v) solution of 3-aminopropyltriethoxysilane (APTES, Sigma) and deionized water (18.2 MΩ Millipore, Billerica, MA, USA) for 5 min followed by a rinse in deionized water. Then two different methods were used to decorate the tip with ssDNA. In the first method, the cantilever was exposed to biotin-labeled bovine serum albumin (BSA, 0.1 μg/mL, Sigma) in a phosphate buffer saline solution (PBS, pH 7.4) for 30 min, rinsed with PBS, and stored at −20 °C for up to 7 days until used. Prior to force spectroscopy measurements, the tips were placed in 40 μL of streptavidin (0.1 μg/mL, S4762, Sigma-Aldrich) in PBS for 30 min at 20 °C, rinsed in PBS, immersed in 40 μL of biotin-labeled ssDNA (IDT) in PBS (at a concentration of 1 μg/mL ssDNA in PBS), and then incubated for another 30 min at 20 °C followed by a final rinse in 100 mM KCl and 10 mM Tris-HCL (pH 8.5) before mounting on the cantilever holder. The force on the frictionless plateaus and rupture force associated with the "slip−stick" transitions are smaller than that required to rupture either the streptavidin−biotin[18−20] or the nonspecific bond between BSA and silicon.[38]

As an alternative to biotin−streptavidin, a second functionalization method used an amine linker to bind the ssDNA to the cantilever. Briefly, following exposure to APTES, a silicon/silicon nitride cantilever was immersed in a 5% (v/v) solution of glutaraldehyde (Amresco, Solon, OH, USA) in PBS for 40 min at 20 °C, followed by a rinse in PBS, and then exposed to a 5′-amine-terminated heteropolymer (poly(C_4T_4)$_{20}$, 1 μg/mL, IDT) for another 40 min. As a final step, sodium cyanoborohydride (4 mM in PBS, Alfa Aesar) was used to reduce the imine bond and stabilize the reaction.

After a topographical scan, with the membrane immersed in electrolyte, the location of the pore was reacquired in either constant force mode (contact mode) or tapping mode by triangulation using the corners of the membrane and high-resolution topology maps imaged with an unfunctionalized tip. In this way, the nanopore was located with a functionalized tip with minimal scanning, thus preserving the DNA on the tip. To measure the force between the nanopore and DNA, the functionalized tip was positioned 30−150 nm above the pore and extended toward the membrane at 10−20 nm/s with a voltage bias applied, while the current, tip deflection, and Z-position were recorded. Contact with the surface resulted in typical tip deflections of 5−10 nm, representing applied forces of 50−500 pN. In addition, to increase the sensitivity, lock-in detection was also used to measure the deflection (5210, Signal

Recovery, Oak Ridge, TN, USA) in response to a 150 μV_{pp} reference signal ac-coupled to the dc trans-membrane bias voltage.

Measurements of the Current Blockade with DNA Tethered to the AFM. The ionic current through a nanopore was measured several ways using either (1) a current-sensing trans-impedance amplifier with a gain of 1×10^6 V/A connected directly to the cantilever holder (Orca, Asylum Research); (2) a patch-clamp amplifier (Axopatch 200B, Molecular Devices) in whole-cell mode; or (3) phase-sensitive lock-in detection (Signal Recovery 5210-Stanford Research) in response to minute periodic changes in the electric field in the nanopore. In each case, Ag/AgCl electrodes embedded in the microfluidic device were used to establish a trans-membrane potential and monitor the pore current. For lock-in detection, the applied dc bias was combined with an ac-signal (100 μV_{pp}) voltage that was used as a reference signal. Each data channel was subsequently sampled at 10 kHz and then digitally filtered using a 250 Hz single-pole Bessel filter (MATLAB).

Signal Autocorrelation Function. Noise in the Z-positional sensor results in multiple measurements for each unique position. Thus, all time series were binned at unique Z-positions spaced every 25 pm, and the mean within each bin was calculated. The spatial autocorrelation of the signal $S_z = \{S_1, S_2, ..., S_N\}$ at lag k was calculated from $AC_kF = 1/N \sum_{z=1}^{N-k} (S_z - \bar{S})(S_{z+k} - \bar{S})$, where $\bar{S}$ represents the mean signal.

Finite Element Simulations (FESs). FESs of the electric field and the electro-osmotic force on the DNA molecule were performed using COMSOL (v4.2a, COMSOL Inc., Palo Alto, CA, USA) following a Poisson−Boltzmann formalism described elsewhere (Figure S2 in the Supporting Information).[22] Briefly, the applied potential ϕ and the potential ψ due to charges on ssDNA and in the nanopore are decoupled from one another and solved independently. The relationship between φ and the charge carriers, K^+ and Cl^-, is given by the Poisson equation $\nabla\varphi = -\rho/\varepsilon\varepsilon_0$, where ρ, ε, and ε_0 are the volume charge density and the relative and vacuum permittivities, respectively. The charge density is given by $\rho = F\sum_i z_i c_i$, where $F = 96\,485$ C/mol is the Faraday constant, z_i is the valence, and c_i is the molar concentrations of ionic species i. The distribution of ions close to charged surfaces satisfies the Boltzmann distribution; thus, the charge density is given by $c_i = c_{0,i} \exp(-z_i e\psi/k_B T)$, where c_0 is the molar concentration far from the DNA/nanopore (*i.e.*, bulk concentration), e is the electric charge, $k_B = 1.38 \times 10^{-23}$ J/K is the Boltzmann constant, and $T = 298$ K is the temperature.

Electro-osmotic flow is expressed by the Navier−Stokes equation, $\eta\nabla^2 u - \nabla p - F\sum_i z_i c_i \nabla V = 0$, where $V = \varphi + \phi$, η is the viscosity, p is the pressure, and u is the velocity. The transport of ionic species is described by the Nernst−Planck equation given by $D_i\nabla^2 c_i + z_i\mu_i c_i \nabla^2 V = u\nabla c_i$, where D is the diffusion coefficient and μ is the ionic mobility. In this treatment, u, V, and c_i are coupled between equations. The relationship between the surface charges σ and the zeta potential ζ is given by the Grahame equation: $\sigma(\zeta) = (8c_0\varepsilon\varepsilon_0 k_B T)^{1/2} \sinh(e\zeta/2k_B T)$.[39] The boundary conditions as defined in Figure S2 for the system are given in Table 1.

The remaining simulation parameters include the density, 1 g cm^{-3}, and viscosity, $\eta = 1.002$ mPa s, of the KCl electrolyte; the diffusion coefficient of K^+, $D_K = 1.33 \times 10^{-5}$ cm^2 s^{-1}, and Cl^-, $D_{Cl} = 2.03 \times 10^{-5}$ cm^2 s^{-1}; the mobility for K^+, $\mu_K = 51.8 \times 10^{-9}$ m^2 V^{-1} s^{-1}, and Cl^-, $\mu_{Cl} = 79.0 \times 10^{-9}$ m^2 V^{-1} s^{-1}; the electrical permittivity, $\varepsilon_0 = 8.85$ pF m^{-1}; the relative permittivity of the electrolyte, $\varepsilon_{el} = 78.5$, and of the silicon nitride membrane, $\varepsilon_{SiN} = 9.7$; the surface charge density of the nanopore, $\sigma = -4$ mC m^{-2} (Figure S6); the ssDNA interbase distance, 0.55 nm, and radius, 0.5 nm; the pore cone angle, $\theta = 20°$; and the membrane thickness, $L_m = 8$ nm.

TABLE 1. Simulation Parameters

boundary	boundary conditions
1: DNA surface	$\sigma = -92.7$ mC m^{-2}; $u = 0$
2: AFM tip	$\sigma = 0$; $u = 0$
3: *trans*-side boundary	$\phi = 0$−1000 mV; $\sigma = 0$; $p = 0$; $c_i = c_0$
4: Si_3N_4 membrane	$\sigma = -4$ mC m^{-2}; $u = 0$
5: *cis*-side boundary	$\phi = 0$; $\sigma = 0$; $p = 0$; $c_i = c_0$

The bare force on an ssDNA molecule of length L_0 and linear charge density λ centered on a nanopore using the axial component of the electric field $E = -\nabla V$ is given by $F_{bare} = \lambda \int_{-L_0/2}^{L_0/2} E_z(r = 0,z)\, dz$. The electro-osmotic force is given by $F_{eom} = 2\pi a\eta \int_{-L_0/2}^{L_0/2} [du_z(r,z)/dr]|_{r=a}\, dz$ where a is the radius of ssDNA. The total effective force is therefore $F_{eff} = F_{bare} - F_{eom}$.

Conflict of Interest: The authors declare no competing financial interest.

Acknowledgment. This work was funded by grants from the National Science Foundation [CCF 1129098 and DBI 1256052] with additional support from a Keough-Hesburgh professorship. We would also like to thank A. Aksimentiev and J. Comer for sharing the results derived from molecular and Brownian dynamics simulations of the translocation of ssDNA and dsDNA prior to publication, and W. Timp, D. Wang, J. Shim, M. Johnson, and K. Sarveswaran for useful discussions.

Supporting Information Available: Figure S1 illustrates conductive AFM measurements of the force performed on a thin (carbon) film resistor. Figure S2 represents the results of FES of the electrophoretic force and electro-osmotic flow in a nanopore. Figure S3 summarizes force and current measurements obtained as DNA was pulled from a silicon nitride surface. Figure S4 shows representative force and current traces associated with the summary in Figure 4. Figure S5 shows TEM and AFM micrographs of the pores used in Figure 6. Finally, we offer a calculation of the charge density of a synthetic nanopore that provides a summary of conductance measurements performed as a function of the KCl electrolyte concentration through a 1×1.2 nm^2 cross-section pore in an 8 nm thick silicon nitride membrane shown in Figure S6. This material is available free of charge *via* the Internet at http://pubs.acs.org.

REFERENCES AND NOTES

1. Mardis, E. R. The Impact of Next-Generation Sequencing Technology on Genetics. *Trends Genet.* **2008**, *24*, 133–141.
2. Pop, M.; Salzberg, S. L. Bioinformatics Challenges of New Sequencing Technology. *Trends Genet.* **2008**, *24*, 142–149.
3. Branton, D.; Deamer, D. W.; Marziali, A.; Bayley, H.; Benner, S. A.; Butler, T.; Di Ventra, M.; Garaj, S.; Hibbs, A.; Huang, X.; Jovanovich, S. B.; Krstic, P. S.; Lindsay, S.; Ling, X. S.; Mastrangelo, C. H.; Meller, A.; Oliver, J. S.; Pershin, Y. V.; Ramsey, J. M.; Riehn, R.; Soni, G. V.; Tabard-Cossa, V.; Wanunu, M.; Wiggin, M.; Schloss, J. A. The Potential and Challenges of Nanopore Sequencing. *Nat. Biotechnol.* **2008**, *26*, 1146–1153.
4. Kasianowicz, J. J.; Brandin, E.; Branton, D.; Deamer, D. W. Characterization of Individual Polynucleotide Molecules Using a Membrane Channel. *Proc. Natl. Acad. Sci. U.S.A.* **1996**, *93*, 13770–13773.
5. Cherf, G. M.; Lieberman, K. R.; Rashid, H.; Lam, C. E.; Karplus, K.; Akeson, M. Automated Forward and Reverse Ratcheting of DNA in a Nanopore at 5-Å Precision. *Nat. Biotechnol.* **2012**, *30*, 344–348.
6. Manrao, E. A.; Derrington, I. M.; Laszlo, A. H.; Langford, K. W.; Hopper, M. K.; Gillgren, N.; Pavlenok, M.; Niederweis, M.; Gundlach, J. H. Reading DNA at Single-Nucleotide Resolution with a Mutant MspA Nanopore and phi29 DNA Polymerase. *Nat. Biotechnol.* **2012**, *30*, 349–353.
7. Pennisi, E. Genome Sequencing. Search for Pore-fection. *Science* **2012**, *336*, 534–537.
8. Sigalov, G.; Comer, J.; Timp, G.; Aksimentiev, A. Detection of DNA Sequences Using an Alternating Electric Field in a Nanopore Capacitor. *Nano Lett.* **2008**, *8*, 56–63.
9. Hyun, C.; Kaur, H.; Rollings, R.; Xiao, M.; Li, J. Threading Immobilized DNA Molecules through a Solid-State Nanopore at >100 μs per Base Rate. *ACS Nano* **2013**, *7*, 5892–5900.

10. Keyser, U. F.; Koeleman, B. N.; Van Dorp, S.; Krapf, D.; Smeets, R. M. M.; Lemay, S. G.; Dekker, N. H.; Dekker, C. Direct Force Measurements on DNA in a Solid-State Nanopore. *Nat. Phys.* **2006**, *2*, 473–477.
11. King, G. M.; Golovchenko, J. A. Probing Nanotube-Nanopore Interactions. *Phys. Rev. Lett.* **2005**, *95*, 216103.
12. Timp, W.; Mirsaidov, U. M.; Wang, D.; Comer, J.; Aksimentiev, A.; Timp, G. Nanopore Sequencing: Electrical Measurements of the Code of Life. *IEEE Trans. Nanotechnol.* **2010**, *9*, 281–294.
13. Lulevich, V.; Kim, S.; Grigoropoulos, C. P.; Noy, A. Frictionless Sliding of Single-Stranded DNA in a Carbon Nanotube Pore Observed by Single Molecule Force Spectroscopy. *Nano Lett.* **2011**, *11*, 1171–6.
14. Mirsaidov, U.; Comer, J.; Dimitrov, V.; Aksimentiev, A.; Timp, G. Slowing the Translocation of Double-Stranded DNA Using a Nanopore Smaller than the Double Helix. *Nanotechnology* **2010**, *21*, 395501.
15. Fologea, D.; Uplinger, J.; Thomas, B.; McNabb, D. S.; Li, J. L. Slowing DNA Translocation in a Solid-State Nanopore. *Nano Lett.* **2005**, *5*, 1734–1737.
16. Storm, A. J.; Storm, C.; Chen, J.; Zandbergen, H.; Joanny, J. F.; Dekker, C. Fast DNA Translocation through a Solid-State Nanopore. *Nano Lett.* **2005**, *5*, 1193–1197.
17. Tabard-Cossa, M.; Wiggin, D.; Trivedi, N. N.; Jetha, J.; Dwyer, R.; Marziali, A. Single-Molecule Bonds Characterized by Solid-State Nanopore Force Spectroscopy. *ACS Nano* **2009**, *3*, 3009–3014.
18. Yuan, C.; Chen, A.; Kolb, P.; Moy, V. T. Energy Landscape of Streptavidin-Biotin Complexes Measured by Atomic Force Microscopy. *Biochemistry* **2000**, *39*, 10219–10223.
19. Rico, F.; Moy, V. T. Energy Landscape Roughness of the Streptavidin-Biotin Interaction. *J. Mol. Recogn.* **2007**, *20*, 495–501.
20. de Odrowaz Piramowicz, M.; Czuba, P.; Targosz, M.; Burda, K.; Szymonski, M. Dynamic Force Measurements of Avidin-Biotin and Streptavdin-Biotin Interactions Using AFM. *Acta Biochim. Polym.* **2006**, *53*, 93–100.
21. Ho, C.; Qiao, R.; Heng, J. B.; Chatterjee, A.; Timp, R. J.; Aluru, N. R.; Timp, G. Electrolytic Transport through a Synthetic Nanometer-Diameter Pore. *Proc. Natl. Acad. Sci. U.S.A.* **2005**, *102*, 10445–10450.
22. Kurz, V.; Nelson, E. M.; Shim, J.; Timp, G. Direct Visualization of Single-Molecule Translocations through Synthetic Nanopores Comparable in Size to a Molecule. *ACS Nano* **2013**, *7*, 4057–4069.
23. Heng, J. B.; Aksimentiev, A.; Ho, C.; Marks, P.; Grinkova, Y. V.; Sligar, S.; Schulten, K.; Timp, G. The Electromechanics of DNA in a Synthetic Nanopore. *Biophys. J.* **2006**, *90*, 1098–1106.
24. Ke, C.; Humeniuk, M.; H, S. G.; Marszalek, P. E. Direct Measurements of Base Stacking Interactions in DNA by Single-Molecule Atomic-Force Spectroscopy. *Phys. Rev. Lett.* **2007**, *99*, 018302.
25. Manohar, S.; Mantz, A. R.; Bancroft, K. E.; Hui, C. Y.; Jagota, A.; Vezenov, D. V. Peeling Single-Stranded DNA from Graphite Surface to Determine Oligonucleotide Binding Energy by Force Spectroscopy. *Nano Lett.* **2008**, *8*, 4365–4372.
26. Saenger, W. *Principles of Nucleic Acid Structure*; Springer-Verlag: New York, 1984.
27. Aksimentiev, A.; Heng, J. B.; Timp, G.; Schulten, K. Microscopic Kinetics of DNA Translocation through Synthetic Nanopores. *Biophys. J.* **2004**, *87*, 2086–2097.
28. Smith, S. B.; Cui, Y.; Bustamante, C. Overstretching B-DNA: the Elastic Response of Individual Double-Stranded and Single-Stranded DNA Molecules. *Science* **1996**, *271*, 795–799.
29. Dessinges, M.-N.; Maier, B.; Zhang, Y.; Peliti, M.; Bensimon, D.; Croquette, V. Stretching Single-Stranded DNA, a Model Polyelectrolyte. *Phys. Rev. Lett.* **2002**, *89*, 248102–248105.
30. Noy, A. Force Spectroscopy 101: How to Design, Perform, and Analyze an AFM-Based Single Molecule Force Spectroscopy Experiment. *Curr. Opin. Chem. Biol.* **2011**, *15*, 710–718.
31. Sulchek, T.; Friddle, R. W.; Noy, A. Strength of Multiple Parallel Biological Bonds. *Biophys. J.* **2006**, *90*, 4686–4691.
32. Baumann, C. G.; Bloomfield, V. A.; Smith, S. B.; Bustamante, C.; Wang, M. D.; Block, S. M. Stretching of Single Collapsed DNA Molecules. *Biophys. J.* **2000**, *78*, 1965–1978.
33. Lu, B.; Hoogerheide, D. P.; Zhao, Q.; Yu, D. Effective Driving Force Applied on DNA Inside a Solid-State Nanopore. *Phys. Rev. E* **2012**, *86*, 011921.
34. Luan, B.; Aksimentiev, A. Electro-osmotic Screening of the DNA Charge in a Nanopore. *Phys. Rev. E* **2008**, *78*, 021912.
35. Bruno, W. J.; Ullah, G.; Mak, D. O.; Pearson, J. E. Automated Maximum Likelihood Separation of Signal from Baseline in Noisy Quantal Data. *Biophys. J.* **2013**, *105*, 68–79.
36. Timp, W.; Comer, J.; Aksimentiev, A. DNA Base-Calling from a Nanopore Using a Viterbi Algorithm. *Biophys. J.* **2012**, *102*, L37–39.
37. Hutter, J. L.; Bechhoefer, J. Calibration of Atomic-Force Microscope Tips. *Rev. Sci. Instrum.* **1993**, *64*, 1868–1873.
38. Florin, E. L.; Moy, V. T.; Gaub, H. E. Adhesion Forces between Individual Ligand-Receptor Pairs. *Science* **1994**, *264*, 415–417.
39. Grahame, D. C. The Electrical Double Layer and the Theory of Electrocapillarity. *Chem. Rev.* **1947**, *41*, 441–501.